Influence of seismic anisotropy on the cross correlation tensor: numerical investigations

M. Saade, J. P. Montagner, P. Roux, Paul Cupillard, S. Durand, F. Brenguier

▶ **To cite this version:**

M. Saade, J. P. Montagner, P. Roux, Paul Cupillard, S. Durand, et al.. Influence of seismic anisotropy on the cross correlation tensor: numerical investigations. Geophysical Journal International, 2015, 201 (2), pp.595-604. 10.1093/gji/ggu470 . hal-01284131

HAL Id: hal-01284131

https://hal.univ-lorraine.fr/hal-01284131

Submitted on 22 Jun 2020

HAL is a multi-disciplinary open access archive for the deposit and dissemination of scientific research documents, whether they are published or not. The documents may come from teaching and research institutions in France or abroad, or from public or private research centers.

L'archive ouverte pluridisciplinaire **HAL**, est destinée au dépôt et à la diffusion de documents scientifiques de niveau recherche, publiés ou non, émanant des établissements d'enseignement et de recherche français ou étrangers, des laboratoires publics ou privés.

Geophysical Journal International

Geophys. J. Int. (2015) **201,** 595–604
GJI Seismology

doi: 10.1093/gji/ggu470

Influence of seismic anisotropy on the cross correlation tensor: numerical investigations

M. Saade,[1] J. P. Montagner,[1] P. Roux,[2] P. Cupillard,[3] S. Durand[4] and F. Brenguier[2]

[1] *Seismology Laboratory, Institut de Physique du Globe de Paris, Paris, France. E-mail: maria.saade90@gmail.com*
[2] *Institut des Sciences de la Terre, University Joseph Fourier, Grenoble, France*
[3] *GeoRessources Laboratory, Nancy School of Geology, University of Lorraine, Vandoeuvre-les-Nancy, France*
[4] *Department of Earth Sciences, École normale supérieure de Lyon, France*

Accepted 2014 December 3. Received 2014 December 2; in original form 2014 March 24

Downloaded from https://academic.oup.com/gji/article-abstract/201/2/595/568214 by guest on 22 June 2020

SUMMARY

Temporal changes in seismic anisotropy can be interpreted as variations in the orientation of cracks in seismogenic zones, and thus as variations in the stress field. Such temporal changes have been observed in seismogenic zones before and after earthquakes, although they are still not well understood. In this study, we investigate the azimuthal polarization of surface waves in anisotropic media with respect to the orientation of anisotropy, from a numerical point of view. This technique is based on the observation of the signature of anisotropy on the nine-component cross-correlation tensor (CCT) computed from seismic ambient noise recorded on pairs of three-component sensors. If noise sources are spatially distributed in a homogeneous medium, the CCT allows the reconstruction of the surface wave Green's tensor between the station pairs. In homogeneous, isotropic medium, four off-diagonal terms of the surface wave Green's tensor are null, but not in anisotropic medium. This technique is applied to three-component synthetic seismograms computed in a transversely isotropic medium with a horizontal symmetry axis, using a spectral element code. The CCT is computed between each pair of stations and then rotated, to approximate the surface wave Green's tensor by minimizing the off-diagonal components. This procedure allows the calculation of the azimuthal variation of quasi-Rayleigh and quasi-Love waves. In an anisotropic medium, in some cases, the azimuth of seismic anisotropy can induce a large variation in the horizontal polarization of surface waves. This variation depends on the relative angle between a pair of stations and the direction of anisotropy, the amplitude of the anisotropy, the frequency band of the signal and the depth of the anisotropic layer.

Key words: Numerical solutions; Seismic anisotropy; Wave propagation.

1 INTRODUCTION

Seismic anisotropy has a key role in the study of strain and stress fields in the Earth. Indeed, on a large scale, the origin of anisotropy (Montagner *et al.* 1998) might be due to the alignment of the crystallographic axes of anisotropic minerals when subjected to a strain field or to aligned cracks (Crampin 1987), or to fluid inclusions, or under the influence of a stress field. As a consequence, the orientation of the anisotropy induced will be parallel to the direction of the stress or strain field that arises through these different processes. Another cause of large-scale anisotropy, and specifically of transverse isotropy with a vertical symmetry axis, is the superposition of thin layers, for wavelengths that are significantly larger than the layer thickness (Backus 1962). In this study, we are interested in seismic anisotropy that is induced by the alignment of cracks in a stress field.

Many methods are used by seismologists to study anisotropy in seismogenic zones, which involve measuring its effects on the propagation of seismic waves. One of these is shear wave splitting (SWS; Vinnik 1977; Crampin *et al.* 1980; Silver & Chan 1991; Zhang *et al.* 2007; Liu *et al.* 2008), a phenomenon that occurs when a polarized shear wave penetrates an anisotropic medium and splits into two *S* waves. Naturally, as with any other technique, SWS has limitations. Indeed, SWS depends on the occurrence of local earthquakes, and it turns out to be difficult to sample all three directions, as most of the shear waves produced by these earthquakes propagate almost vertically. These limitations to the monitoring of seismic anisotropy can be alleviated by using cross-correlations of continuous ambient noise between each pair of stations in a network of stations, according to the three components of vertical (Z), east and north, rotated into vertical (Z), radial (R) and transverse (T).

© The Authors 2015. Published by Oxford University Press on behalf of The Royal Astronomical Society.

The cross-correlation tensor (CCT) computed between two three-component (Z, R, T) seismograms at two different receivers (A, B) is an estimation of the transfer function (Green's function) between these receivers. The CCT has nine components that represent all of the possible cross-correlations between the three component signals recorded at the two receivers. For a homogeneous random distribution of noise sources, the CCT represents the impulse response of the Earth between these two stations. In practice, however, the CCT is dominated by surface waves. Unlike the vertically propagating shear waves that are used for SWS, surface waves propagate horizontally. This allows the measurement of the horizontal seismic properties in the shallow crust.

Since their application to seismology in 2004, the use of the ZZ components of the CCT has enabled the imaging of seismic velocity subsurface structures from seismic ambient noise. The monitoring of seismic velocity changes, which might be related to stress changes in seismogenic zones, has also been demonstrated, with computation of the relative traveltime shift between a perturbed and a reference ZZ for each station pair (Brenguier *et al.* 2008).

Another technique is based on the investigation of the off-diagonal terms of the CCT: ZT, TZ, RT and TR. Indeed, for a random distribution of seismic sources, these non-diagonal terms are null in an isotropic medium. However, in an anisotropic medium, they are no longer null; that is, the polarization plane of quasi-Rayleigh waves is deviated with respect to the isotropic case, and the polarization of quasi-Love waves is no longer in the horizontal plane. The surface wave polarizations are no longer parallel or perpendicular to the direction of propagation. Their directions are slightly deviated, which creates quasi-Rayleigh and quasi-Love waves (Crampin *et al.* 1980). If the CCT is rotated to minimize the off-diagonal components with the optimal rotation algorithm (ORA) code (Roux 2009), the deviation anomaly angles (ψ, δ) at both receivers (A and B) can be retrieved. These four angles are defined by the horizontal polarization anomaly at receivers A and B (ψ_A, ψ_B) and the vertical polarization anomaly at receivers A and B (δ_A, δ_B). These anomaly angles inform us about the anisotropic properties in the medium or the inhomogeneity of sources (Durand *et al.* 2011).

In this study, a numerical investigation is performed, knowing that there is no analytical solution for surface wave propagation in such anisotropic medium with horizontal symmetry axis. Our goal is to investigate the physical conditions that can give rise to rotation of the polarization of seismic surface waves, and it is the most efficient way to measure the azimuthal rotation that is linked to anisotropy. The objective is to correctly interpret the observations made by Durand *et al.* (2011) for large variations in surface wave polarization ($>20^\circ$) within a limited zone of the seismic array, and before and after the 2004 Parkfield earthquake. In the following, the technique based on the optimal rotation of noise cross-correlation is detailed and then tested on synthetic seismograms that are computed with a spectral element method [the RegSEM code, for the regional spectral elements method, as detailed in Cupillard *et al.* (2012)].

2 SYNTHETIC EXPERIMENTS

The goal is to quantitatively investigate the influence of anisotropy on the wave propagation, by observing the azimuthal change of the wave polarization and the phase velocity according to the direction of incidence of the source. The RegSEM code allows the numerical computation of accurate synthetic seismograms in heterogeneous anisotropic 3-D earth models. As it can handle any kind of anisotropy, RegSEM enables us to investigate the influence of the

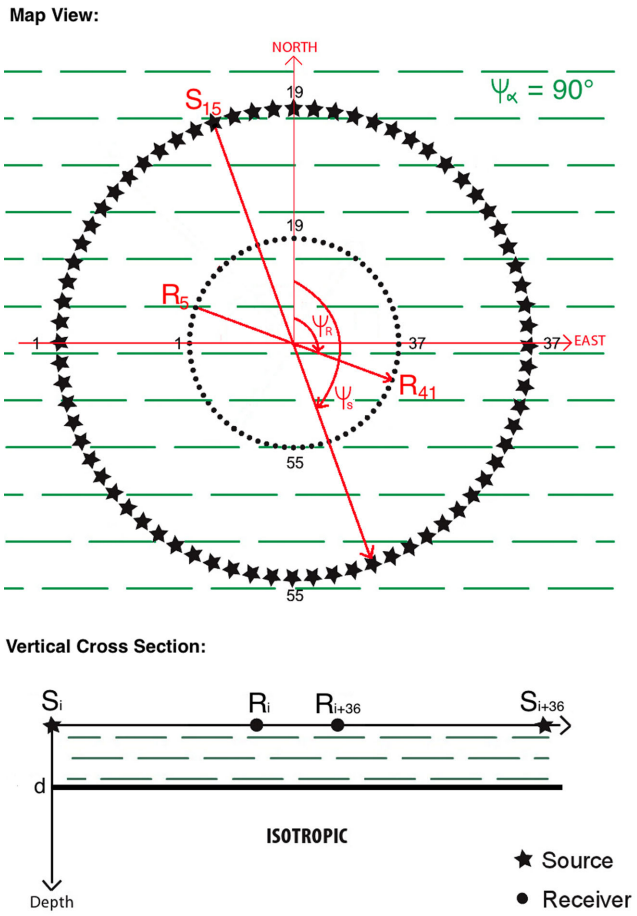

Figure 1. Representation of the HTI medium, the 72 sources, and the 72 stations. This figure is not drawn to scale [$\Delta(R_1 - R_{37}) = 10$ km and $\Delta(S_1 - S_{37}) = 332$ km]. ψ_α is the azimuth of the fast direction of anisotropy fixed in the east–west direction, ψ_S is the azimuth of incidence of the source, and ψ_R is the azimuth of the pair of stations. All angles are measured in degrees in a clockwise direction from the north line.

input parameters and to perform realistic simulations. In this study, all of the synthetic data result from simulations provided in a section of the earth (700 × 700 × 100 km). We designed a numerical experiment where the medium is defined as a superposition of two homogeneous layers (Fig. 1). In fact, the model is constructed in a way to be more realistic than the simplest one-layer homogeneous medium. The bottom layer is isotropic, in which the elastic tensor C^{iso} has only two independent terms, λ and μ, which are called the Lamé coefficients; using Voigt notation, the elastic 6 × 6 matrix can be written as:

$$C^{\text{iso}} = \begin{pmatrix} \lambda+2\mu & \lambda & \lambda & 0 & 0 & 0 \\ \lambda & \lambda+2\mu & \lambda & 0 & 0 & 0 \\ \lambda & \lambda & \lambda+2\mu & 0 & 0 & 0 \\ 0 & 0 & 0 & \mu & 0 & 0 \\ 0 & 0 & 0 & 0 & \mu & 0 \\ 0 & 0 & 0 & 0 & 0 & \mu \end{pmatrix}. \quad (1)$$

In this layer, the isotropic *P*- and *S*-wave velocities are constants, and are, respectively, defined by:

$$V_p = \sqrt{\frac{\lambda+2\mu}{\rho}}, \quad (2)$$

Downloaded from https://academic.oup.com/gji/article-abstract/201/2/595/568214 by guest on 22 June 2020

and

$$V_s = \sqrt{\frac{\mu}{\rho}}, \tag{3}$$

The top layer is a transversely isotropic medium with a horizontal symmetry axis (HTI); the fast direction of anisotropy is arbitrarily set as east to west. The anisotropy in this layer results from the existence of five elastic constants, known as A, C, F, L and N, in the elastic tensor C^{HTI}. Hence the HTI (anisotropic) layer is defined by the input of these five elastic moduli in the RegSEM code. Assuming direction 1 to be the east–west direction, the elastic tensor C^{HTI} can be written as (Anderson 1989):

$$C^{\mathrm{HTI}} = \begin{pmatrix} C & F & F & 0 & 0 & 0 \\ F & A & A-2N & 0 & 0 & 0 \\ F & A-2N & A & 0 & 0 & 0 \\ 0 & 0 & 0 & N & 0 & 0 \\ 0 & 0 & 0 & 0 & L & 0 \\ 0 & 0 & 0 & 0 & 0 & L \end{pmatrix}. \tag{4}$$

where:

$$A = \rho V_{PH}^2, \tag{5}$$

$$C = \rho V_{PV}^2, \tag{6}$$

$$L = \rho V_{SV}^2, \tag{7}$$

$$N = \rho V_{SH}^2 \tag{8}$$

and

$$F = \eta(A - 2L). \tag{9}$$

Indeed, V_{PH}, V_{PV}, V_{SV} and V_{SH} refer to a vertical transverse isotropy model that is then rotated by 90° around the north–south axis, to produce a HTI model. The amplitude of anisotropy in the model is based on the input of the A, C, F, L and N parameters. These parameters represent the directional dependence of the velocities of the seismic waves. In the half-space bottom layer, we define the isotropic velocities as $V_P = 6.75\,\mathrm{km\,s^{-1}}$, $V_S = 3.85\,\mathrm{km\,s^{-1}}$ and $\rho = 3000\,\mathrm{kg\,m^{-3}}$. As for the top layer, the anisotropic velocities are defined by:

$$V_{PH} = V_P(1 - a), \tag{10}$$

$$V_{PV} = V_P(1 + a), \tag{11}$$

$$V_{SH} = V_S(1 - a) \tag{12}$$

and

$$V_{SV} = V_S(1 + a). \tag{13}$$

where a is the velocity anomaly due to anisotropy; for example, in a ±10 per cent anisotropic medium, $a = 0.1$. Moreover, $\eta = 1.1$ and $\rho = 3000\,\mathrm{kg\,m^{-3}}$. As indicated in Fig. 1, 72 sources S_S and 72 receivers R_R on the surface are distributed in two concentric circles. This configuration allows us to explore all of the possible azimuthal positions of the source (ψ_S) and the stations (ψ_R), with respect to the direction of anisotropy (ψ_α). Each source is an impulse that is defined by a vertical force, and that covers the frequency range of 2.5–20 s. The sources are located far from the receivers, which facilitates the study, as we can easily separate body waves from surface waves. The duration of each seismogram is 200 s and the sampling rate is 10 Hz. No attenuation is considered in the model. Four different angles are explored (Fig. 1): ψ_α, which defines the azimuth of the fast direction of anisotropy fixed in the east–west direction; ψ_S, which defines the azimuth of the incidence of the source; ψ_R, which defines the azimuth of the pair of stations and ψ_P, which is the polarization anomaly angle. ψ_S, ψ_R, and ψ_P are measured in degrees in a clockwise direction from the north line.

We start by considering the case of an impulse force at the source location, so the transformation of the Rayleigh wave into a quasi-Rayleigh wave will be correctly observed, limiting the influence of the Love wave. That way we can clearly explore the effect of anisotropy on the propagation of Rayleigh waves only. Fig. 2 shows that the signal on the radial and vertical components of the synthetic seismograms is dominated by Rayleigh waves in isotropic and anisotropic media.

Fig. 2 also shows that a weak signal appears on the transverse component for waves that propagate in an anisotropic medium, which is primarily due to the deviation of the Rayleigh wave into a quasi-Rayleigh wave. There is also a small faster signal that might be related to quasi-Love waves. The anisotropy affects the group velocity: there is a decrease in the group velocity when the azimuth of incidence of the source ψ_S approaches the north-south direction. This is the minimum for a wave that propagates perpendicular to the direction of anisotropy, where the velocity is slowest, and the group velocity is maximum for a wave propagating along the direction of anisotropy. Another observation is the difference between the velocities along the fast axis and the slow axis, which is 20 per cent, the percentage of anisotropy in the top layer (±10 per cent).

3 THE METHOD

3.1 Cross-correlation of seismic data

We first compute the CCT between two three-component seismograms computed using the RegSEM code for station pairs (A and $B = A + 36$; i.e. the receivers are located on a diameter of the inner circle in Fig. 1) with azimuth ψ_R. The CCT is a nine-component tensor $C^G_{AB}(t)$ computed in geographical coordinate system G (vertical, east, north), for each station pair (A and B). The usual normalized cross-correlation formula (Shapiro *et al.* 2006; Brenguier *et al.* 2008) is given by:

$$\left[C^G_{AB}(t)\right]_{ij} = \frac{\int_0^{\Delta T} S_{A,i}(\tau) S_{B,j}(t+\tau)\mathrm{d}\tau}{\sqrt{\int_0^{\Delta T} S^2_{A,i}(\tau)\mathrm{d}\tau \int_0^{\Delta T} S^2_{B,j}(\tau)\mathrm{d}\tau}}, \tag{14}$$

where each component of the CCT is normalized with respect to its own energy. However, this normalization is no longer valid in the presence of seismic anisotropy, as some field contributions are transferred from one component to another. In this case, each component of the CCT should be normalized with respect to the total energy:

$$\left[C^G_{AB}(t)\right]_{ij} = \frac{\int_0^{\Delta T} S_{A,i}(\tau) S_{B,j}(t+\tau)\mathrm{d}\tau}{\sqrt{\int_0^{\Delta T} \sum_i S^2_{A,i}(\tau)\mathrm{d}\tau \int_0^{\Delta T} \sum_j S^2_{B,j}(\tau)\mathrm{d}\tau}}, \tag{15}$$

Downloaded from https://academic.oup.com/gji/article-abstract/201/2/595/568214 by guest on 22 June 2020

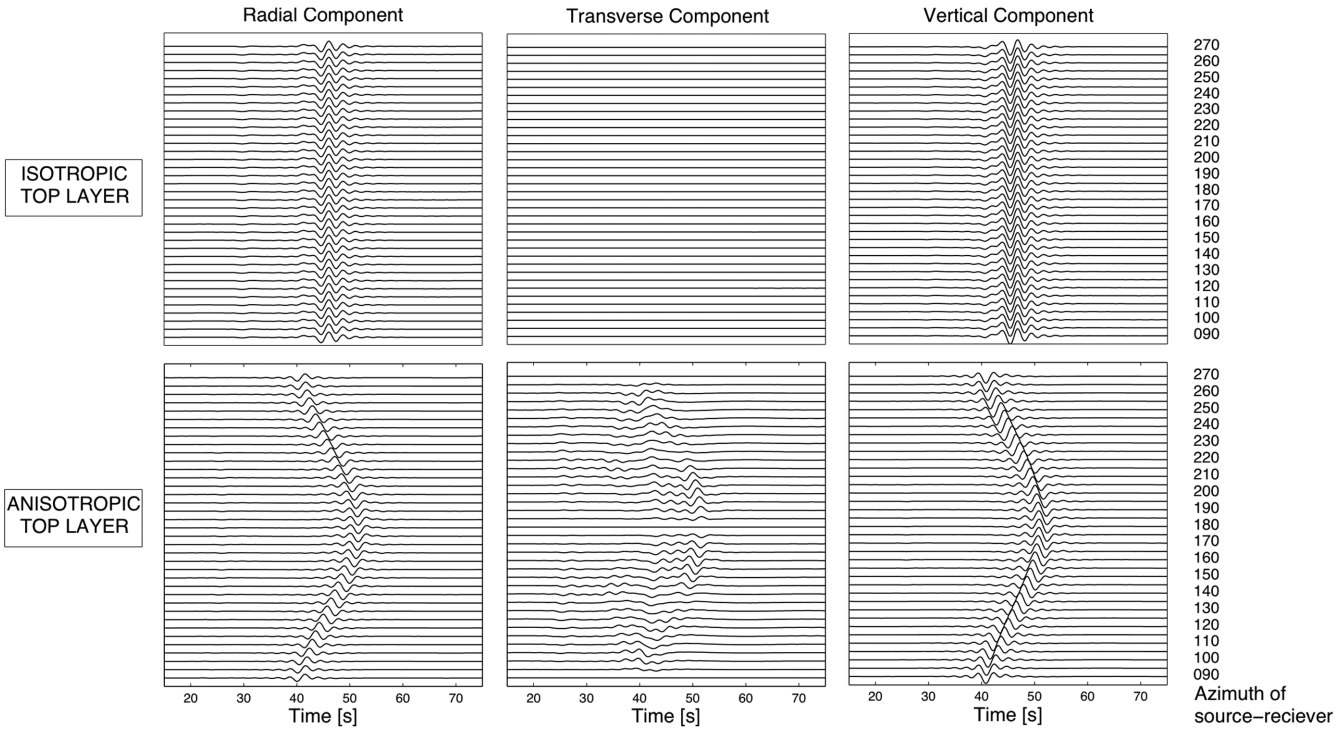

Figure 2. Radial, transverse and vertical components for the source incidences, going from azimuth 90° to 270°. The source–station pairs that correspond to the different azimuths are formed from sources S_i and receivers R_i located on the circles shown in Fig. 1; for example, for azimuth 135°, the source is S_{10} and the receiver is R_{10}. As indicated, the top three panels are seismograms computed in an isotropic medium, and the bottom three panels are seismograms that were computed in a medium where the velocity anisotropy is ±10 per cent and the thickness d of the top anisotropic layer is 10 km. In the isotropic medium, there are only Rayleigh waves on the radial and vertical components. In the anisotropic medium, and for waves that propagate along the fast and slow axes (90°, 180°), there are also only Rayleigh waves on the radial and vertical components, which propagate in the symmetry planes of the medium. However, for the other source incidences, a signal appears on the transverse component, which is due to the creation of quasi-Rayleigh wave in the anisotropic medium. Moreover, in the anisotropic medium, the group velocity decreases as the incidence of the source approaches the slow axis, and increases as the incidence of the source approaches the fast axis.

where $S_{A,i}(t)$ and $S_{B,i}(t)$ are the vertical or horizontal components of the signal at stations A and B, 'i' defines the component (Z, E or N). ΔT represents the recording time window on which the correlation is performed. The nine components of the CCT are ZZ, ZE, ZN, EZ, EE, EN, NZ, NE and NN, as defined by the geographical coordinate system (Z, E, N) which can be transformed into the station-pair coordinate system (Z, R, T) such that the CCT components are now ZZ, ZR, ZT, RZ, RR, RT, TZ, TR and TT, where the radial axis R is parallel to the station-pair direction defined by its azimuth, and the transverse axis T is perpendicular to this. The CCT is then:

$$C_{AB} = \begin{pmatrix} \text{ZZ} & \text{ZR} & \text{ZT} \\ \text{RZ} & \text{RR} & \text{RT} \\ \text{TZ} & \text{TR} & \text{TT} \end{pmatrix}. \tag{16}$$

In the case of the omnidirectional surface noise sources, the CCT is the sum of causal and 'anticausal' contributions that correspond to advanced and delayed surface wave Green's functions between two stations (Sabra *et al.* 2005; Roux 2009). However, in practice, the noise distribution is often directive, or at least, not omnidirectional. In the case of directive noise, as in Parkfield (Durand *et al.* 2011; Roux 2009), everything happens as if only one source direction (defined by the dominant energy source) is active in the far field of the receivers, which results in asymmetric correlation functions on each component of the CCT, as shown in Fig. 3.

3.2 Application of the optimal rotation algorithm

The ORA was first introduced in Roux (2009), to deal with directive incident noise for seismic noise tomography. In fact, in order to perform passive seismic imaging, station pairs that do not align with the noise direction should be thrown away, since they provide a biased traveltime through noise correlation (Roux 2009). The main objective of ORA is to allow each station (from a specific station pair, A and B) to freely rotate around both the vertical axis (with the azimuth angle ψ) and the radial axis (with the tilt angle δ) and to align with the incident noise direction (Fig. 4), by minimizing the four off-diagonal terms ZT, RT, TZ and TR of the CCT computed between these two stations (Fig. 3c). This way, the number of station pairs that can be used in the traveltime tomography inversion is increased.

For every set of angles (ψ_A, ψ_B) and (δ_A, δ_B) that are associated with stations A and B, the ORA computes the new rotated CCT, $C'_{AB}(t)$. For each new CCT, the ORA calculates a misfit parameter M, which is defined as:

$$M(\psi_A, \psi_B, \delta_A, \delta_B) = \frac{\left[C'^{\,2}_{AB}\right]_{13} + \left[C'^{\,2}_{AB}\right]_{23} + \left[C'^{\,2}_{AB}\right]_{31} + \left[C'^{\,2}_{AB}\right]_{32}}{\sum_{k=1}^{3}\sum_{l=1}^{3}\left[C'^{\,2}_{AB}\right]_{kl}}, \tag{17}$$

where k and l are the R, T and Z components of the new CCT, as $1 = Z$, $2 = R$ and $3 = T$. $[C'_{AB}]_{kl}$ is the new cross-correlation

Downloaded from https://academic.oup.com/gji/article-abstract/201/2/595/568214 by guest on 22 June 2020

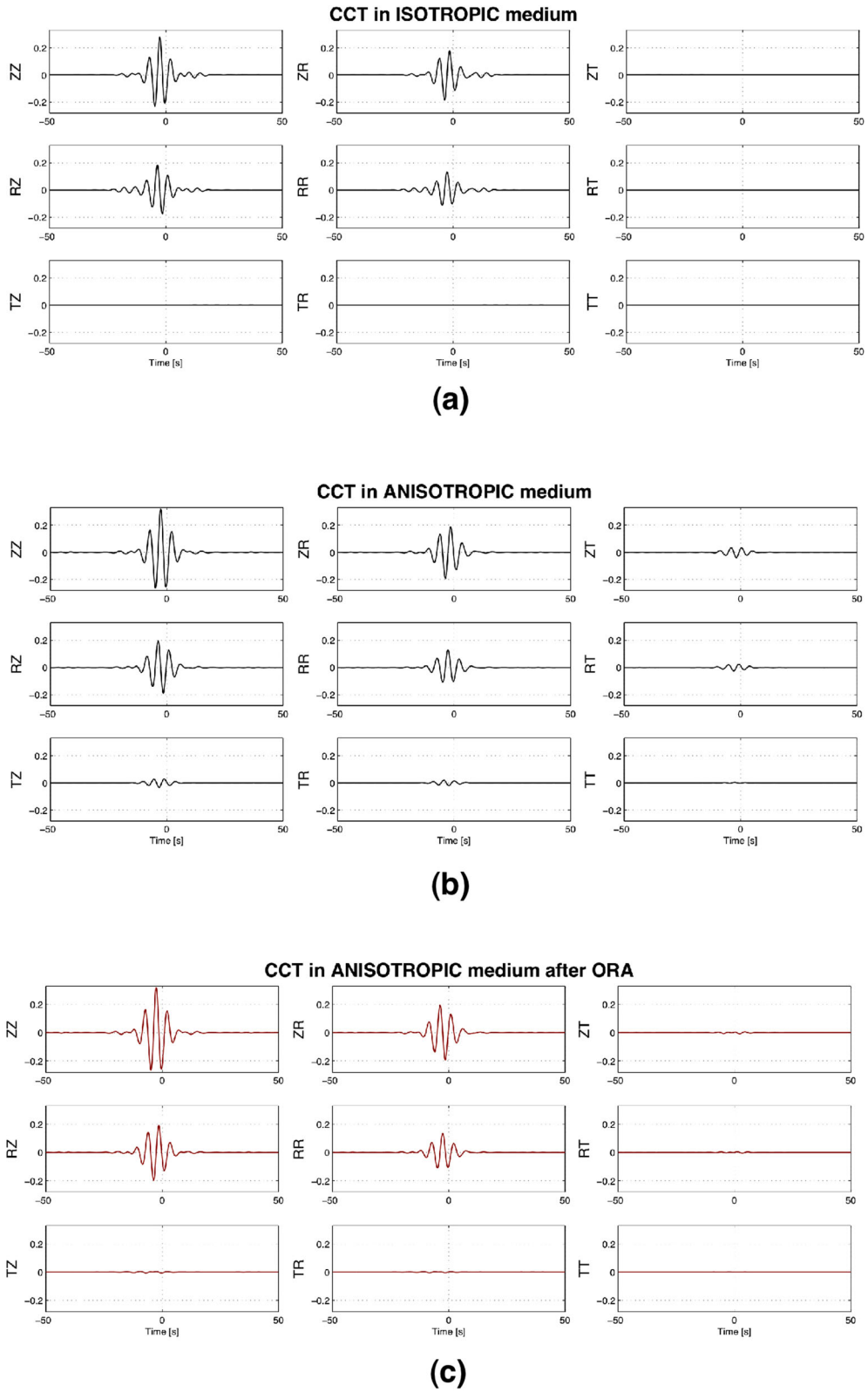

Figure 3. (a) CCT in an isotropic medium for a single source and a receiver pair of azimuth 110°. (b) CCT for the same receiver pair in an anisotropic medium, where the velocity anisotropy is ±10 per cent. (c) CCT after the application of the ORA. The frequency band in all cases is 0.15–0.25 Hz. The source is aligned with the pair of stations, and the CCTs are represented in the ZRT coordinate system, where the radial axis is parallel to the incidence of the source.

Downloaded from https://academic.oup.com/gji/article-abstract/201/2/595/568214 by guest on 22 June 2020

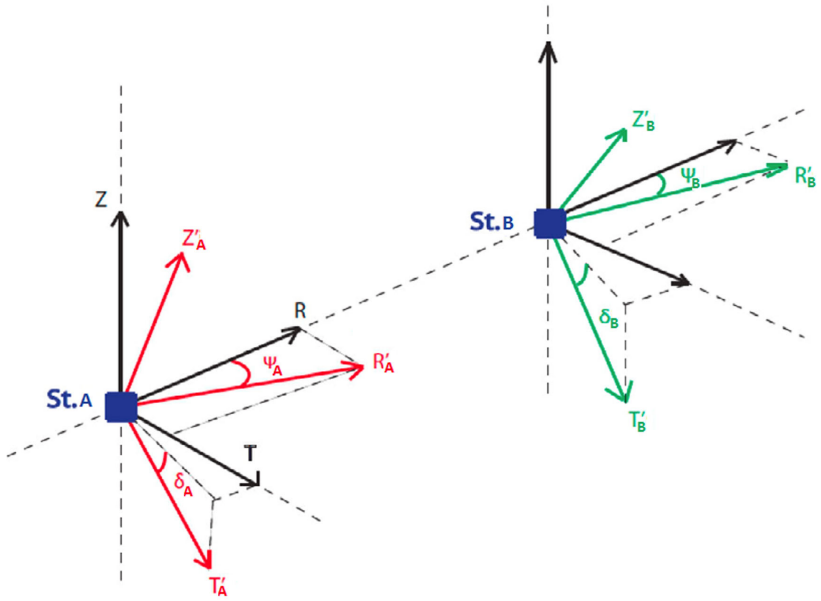

Figure 4. Azimuths ψ_A and ψ_B and tilts δ_A and δ_B used in the ORA.

function between the component k of station A and the component l of station B.

The ORA is then used to determine the set of angles that minimizes the components ZT, RT, TZ and TR of the original CCT, by finding the minimum misfit parameter. Indeed, the less M is, the closer the tensor is to the Rayleigh wave Green's tensor.

Thus, even if the station pair is originally misaligned with the noise incidence, the four off-diagonal terms ZT, RT, TZ and TR, will be zeros after the ORA rotation, if we assume the medium is isotropic. In this way, it is possible to correct the station pairs that do not align with the noise direction by rotating both stations and to provide unbiased tomography measurements through noise correlation (Roux 2009). However, Fig. 3(b) shows that in the case of an anisotropic medium, components ZT, RT, TZ and TR still have nonzero values; that is, the polarization plane of the quasi-Rayleigh and quasi-Love waves is slightly deviated by horizontal and vertical angles, with respect to the polarization plane of the Rayleigh and Love waves in the isotropic medium.

In this case, the value of the ORA azimuthal rotation angle that minimizes the components ZT, RT, TZ and TR of the CCT is equal to the angle that aligns the station pairs with the noise source incidence and an additional angle that is due to the deviation of the Rayleigh and Love waves in the anisotropic medium (Fig. 3c). Our goal is to investigate this additional rotation angle that arises due to the anisotropy, by using ORA in cases where the station pairs are aligned with the source incidence. Therefore, the difference between the azimuthal rotation angles given by ORA (ψ_A, ψ_B) and the azimuth of the source incidence gives the anomaly angles that are associated with the deviation of the surface waves in an anisotropic medium at both stations. Here ψ_A is equal to ψ_B because the source is aligned with the stations pair, hence the anomaly angle is the same at both stations. The case of omnidirectional source distribution is presented in Fig. 5, for which the anomaly angle becomes independent of the source incidence.

4 RESULTS

In the numerical experiment, the CCT is computed for each pair of stations, as stations R_i and R_{i+36}, which are aligned along the diameter of the inner circle shown in Fig. 1 (dots). The Rayleigh wave sources are distributed in the far field of the receivers in a circle of radius 166 km, as shown in Fig. 1 (stars). The polarization anomaly angles ψ_P and δ_P computed using the ORA are functions of ψ_R. We note that the tilt δ_P is always negligible, as the medium is HTI, and hence we study only the azimuthal polarization anomaly ψ_P. Fig. 6 shows the variation of the horizontal polarization anomaly (ψ_P) for different frequency bands. In the model, the depth of the anisotropic layer is 10 km, and the amplitude of anisotropy is $\pm$10 per cent.

First of all, the point sources are studied one by one, and we consider the case where the azimuth of the source ψ_S is equal to the azimuth of the station pair ψ_R. For the direction source stations parallel or perpendicular to the direction of anisotropy (fast or slow axis for propagation of the signal in a symmetry plane), there is no transverse component and no effects of anisotropy, except through the propagation velocity. Hence, the terms ZT, RT, TR and TZ of the CCT are null, and so the angle given by the ORA is equal to the azimuth of the station pair. On the contrary, as soon as the angle between the direction source stations and the direction of anisotropy is different from 0° or 90°, the anisotropy affects the wave propagation and the polarization anomaly can be computed. Looking at the results for a single point source and two symmetrical sources, a first observation is that ψ_P appears to be highly dependent on the frequency band, and basically varies with 2Ψ and 4Ψ (Fig. 6 a). This frequency dependence is due to the presence of anisotropy in the shallow layer.

Note also that the azimuthal variation of the tilt δ_P (the vertical polarization anomaly angle) has small values comparing to ψ_P. The tilt δ_P, can be ignored, as expected for a HTI medium. This will not be the case for a tilted transversely isotropic medium, which might be the case in subduction zones.

The third case is a simulation of a homogeneous azimuthal distribution of far-field sources by adding the contribution of all of the sources on the external circle. For each station pair, a stack of the individual CCTs obtained from the 72 sources is almost equivalent to the CCT obtained in a uniform source distribution, which leads to the reconstruction of the surface wave Green's tensor. We then observe the variation of the horizontal polarization anomaly angle

Downloaded from https://academic.oup.com/gji/article-abstract/201/2/595/568214 by guest on 22 June 2020

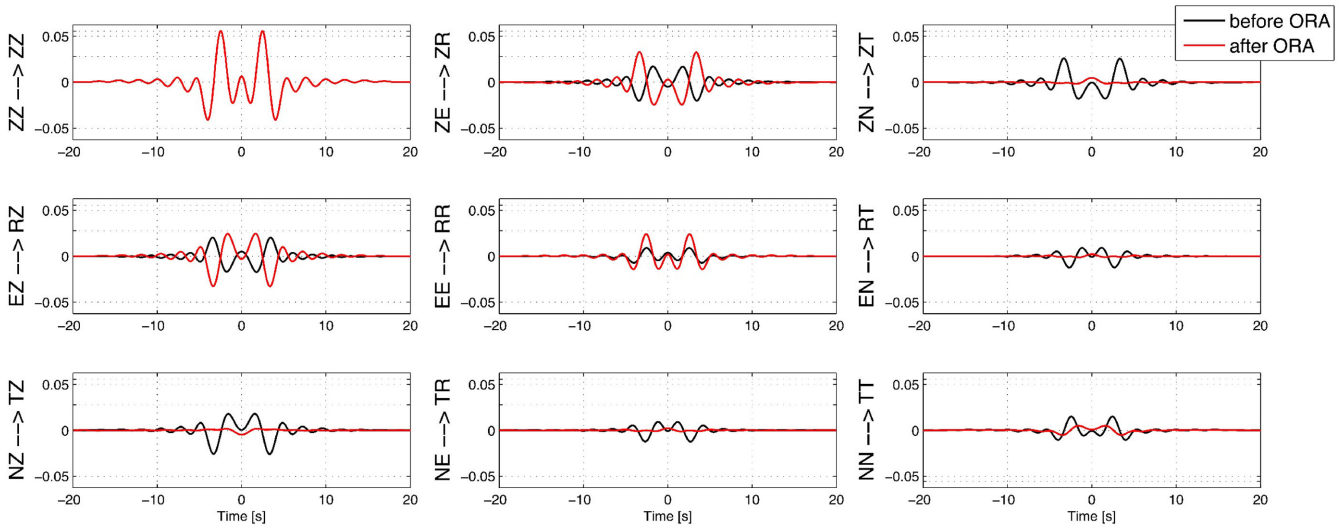

Figure 5. Representation of the CCT before (black) and after (red) the ORA, for a receiver pair of azimuth 135°. This is a case of multidirectional far sources in a ±10 per cent anisotropic medium.

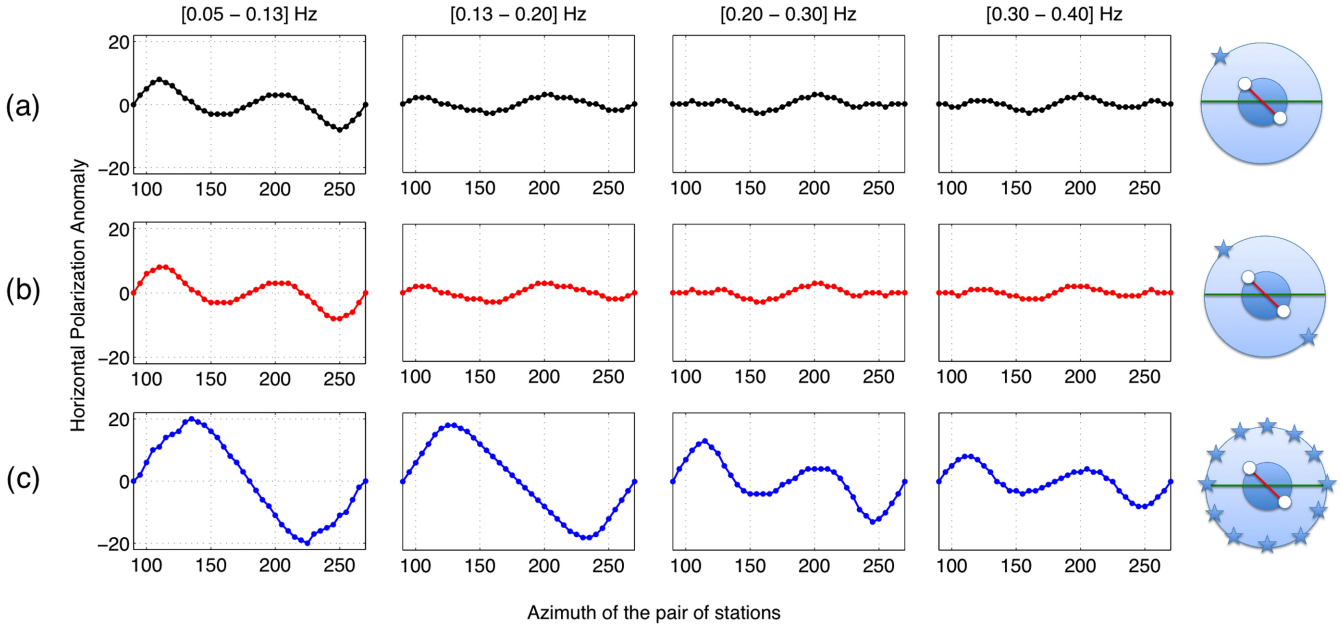

Figure 6. Variations in the horizontal polarization anomaly angle ψ_P as a function of ψ_R for three cases: a point source ($\psi_S = \psi_R$) (black), two symmetrical sources (red), and the stack of the CCTs of all of the sources (blue). In this model, the depth of the anisotropic layer is 10 km, and the anisotropy is ±10 per cent.

ψ_P as a function of the azimuth of the station pair ψ_R. In this case, the variations of ψ_P are larger and vary with 2Ψ at lower frequencies. Between 0.17 and 0.25 Hz, the sign of ψ_P begins to reverse, with 2Ψ and 4Ψ variations (Fig. 6c).

Based on the study of Tanimoto (2004), theory shows that the polarization of surface waves propagating in an anisotropic medium contains 2Ψ and 4Ψ azimuthal dependance, similar to the phase velocity variations. In particular in an HTI medium, it is possible to detect azimuthal dependance of 2Ψ and 4Ψ in the azimuthal polarization of surface waves. 4Ψ variations are basically related to Love waves, whereas 2Ψ variations are related to Rayleigh waves that seem to be dominating at lower frequencies where sources are homogeneously distributed.

Another observation is the difference between the results with a single point source and a homogeneous distribution of sources. Indeed, the present study shows that the sum of the CCTs in an anisotropic medium is different from the sum in an isotropic one. In an isotropic medium, contributions to the CCTs from antisymmetric sources ($S_{i+k} - S_{i-k}$, where i is from 1 to 72 and k is from 1 to 35 and they define the location of the source as in Fig. 1) cancel each other out in the summation. The result would be a surface wave Green's tensor equivalent to the tensor built by the sum of two CCTs associated with the two symmetrical sources on either side of the station pair. However, in an anisotropic medium, the sum is different. These same contributions have different arrival times, so they do not vanish after the summation.

Finally, note that the amplitude of the polarization anomaly ψ_P can be very large (reaching 20° and more), and it depends on many parameters, such as the amplitude of anisotropy and the frequency of the signal.

As mentioned previously, the final CCT obtained after the rotation using the ORA is the one that corresponds to the lowest misfit. Fig. 7

Downloaded from https://academic.oup.com/gji/article-abstract/201/2/595/568214 by guest on 22 June 2020

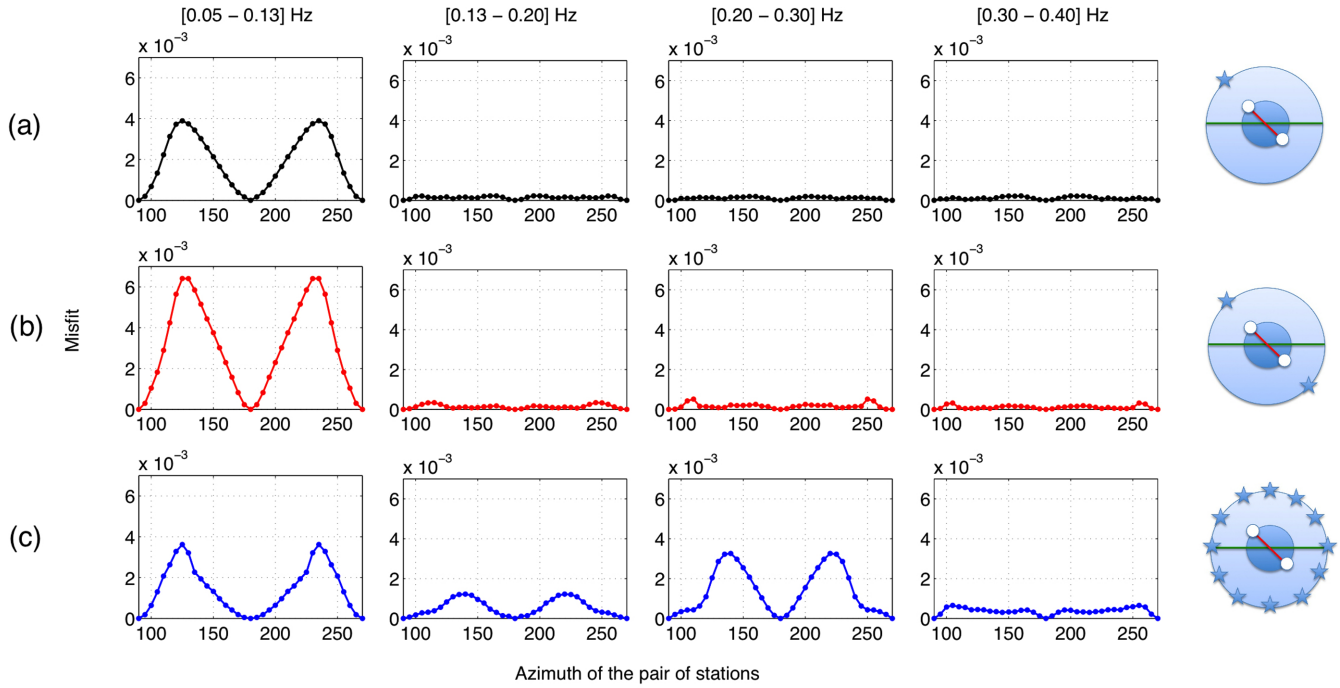

Figure 7. Final misfit obtained from the ORA as a function of ψ_R, and corresponding to the computation of the horizontal polarization anomaly in the three cases shown in Fig. 6: a point source ($\psi_S = \psi_R$) (black); two symmetrical sources (red); and a stack of the CCTs of all of the sources (blue). As shown in the figure, the misfit should be less than 1 per cent of the total energy.

shows the value of the final misfit given by the ORA as a function of ψ_R, for each CCT rotated and horizontal polarization anomaly computed. In Fig. 7, the three cases from Fig. 6 are represented, including a single point source ($\psi_S = \psi_R$), two symmetrical sources, and a stack of the CCTs of all of the sources. The value of the final misfit for all of the cases is <1 per cent of the total energy, which validates the use of the ORA.

5 DISCUSSION

In the crust, the occurrence of an earthquake affects and rotates the stress tensor. Consequently, the temporal rotation of the stress tensor induces rotation of the crack distribution (Crampin 1981), and hence a change in the direction of the anisotropy (ψ_α), which induces temporal changes in the polarization of the surface waves propagating in the medium (ψ_P). ψ_P depends on the relative angle between the azimuth of the station pair and the direction of the anisotropy, $\psi_R - \psi_\alpha = \Delta_\psi$. In 'real life', we search for temporal changes in $\psi_\alpha(t)$ by monitoring $\psi_P(t)$, knowing ψ_R. In our numerical experiments, we investigated the variation of ψ_P with fixed ψ_α in the east–west direction, and we considered various ψ_R. The positions of the source and the station pair vary, spanning the whole range of azimuthal incidences relative to the direction of anisotropy. In this way, it is possible to observe the azimuthal variation of the horizontal polarization anomaly angle ψ_P, measured using the ORA, as a function of ψ_R, the azimuth of the path. Therefore spatial variations observed with synthetic tests can be interpreted in terms of temporal variations observed with real data, given the equivalence between the two.

The results of the numerical experiments combined with the theory of anisotropic wave propagation show that the variation of the horizontal polarization of a surface wave propagated in an anisotropic medium (and here we consider a HTI medium) greatly depends on several parameters. These parameters are the amplitude of anisotropy, the depth and thickness of the anisotropic layer, the distance between the source and the receivers, and especially the azimuth of the source and the pair of receivers relative to the azimuth of anisotropy. Another parameter is the homogeneity of the source distribution. The CCT converges toward the Green's tensor if the source distribution is uniform. This is rarely the case; that is, in the region of California, the main source of noise originates along the Californian coast at short periods, but from the northern Atlantic at long periods, as shown by Stehly *et al.* (2006).

The goal of this paper is not to demonstrate the Green's function reconstruction between two receivers, which was done in earlier papers for any level of heterogeneity in the propagation medium (Campillo & Roux 2014). The goal here is to search for the effect of anisotropy from an interferometric approach. In fact we deal with far-away sources and we chose pairs with small interstation distances. That way we have a good coherence between receivers and we study local effects beneath the stations. As in the case of Parkfield (Durand *et al.* 2011), large polarization changes were observed although interstation distances are relatively small. Note also, that the effect of anisotropy on the propagation of surface waves is not cumulative, unlike traveltime measurements. It depends on the anisotropic structure of the medium but not on the distance travelled by the wave.

As a matter of fact, the level of complexity that interests us and that we want to address in this study is the one related to the anisotropic model, and not to the complexity related to the source distribution. Therefore, we use the most favourable cases, an homogeneous distribution of sources as well as directive noise sources as found in Parkfield (Durand *et al.* 2011) but still aligned with the receiver pair. That is why the azimuthal polarization anomaly at both receivers is the same. If we consider an heterogeneous source distribution, the only difference is that the polarization anomaly will be different at each receiver. In real case scenario, the heterogeneity

Downloaded from https://academic.oup.com/gji/article-abstract/201/2/595/568214 by guest on 22 June 2020

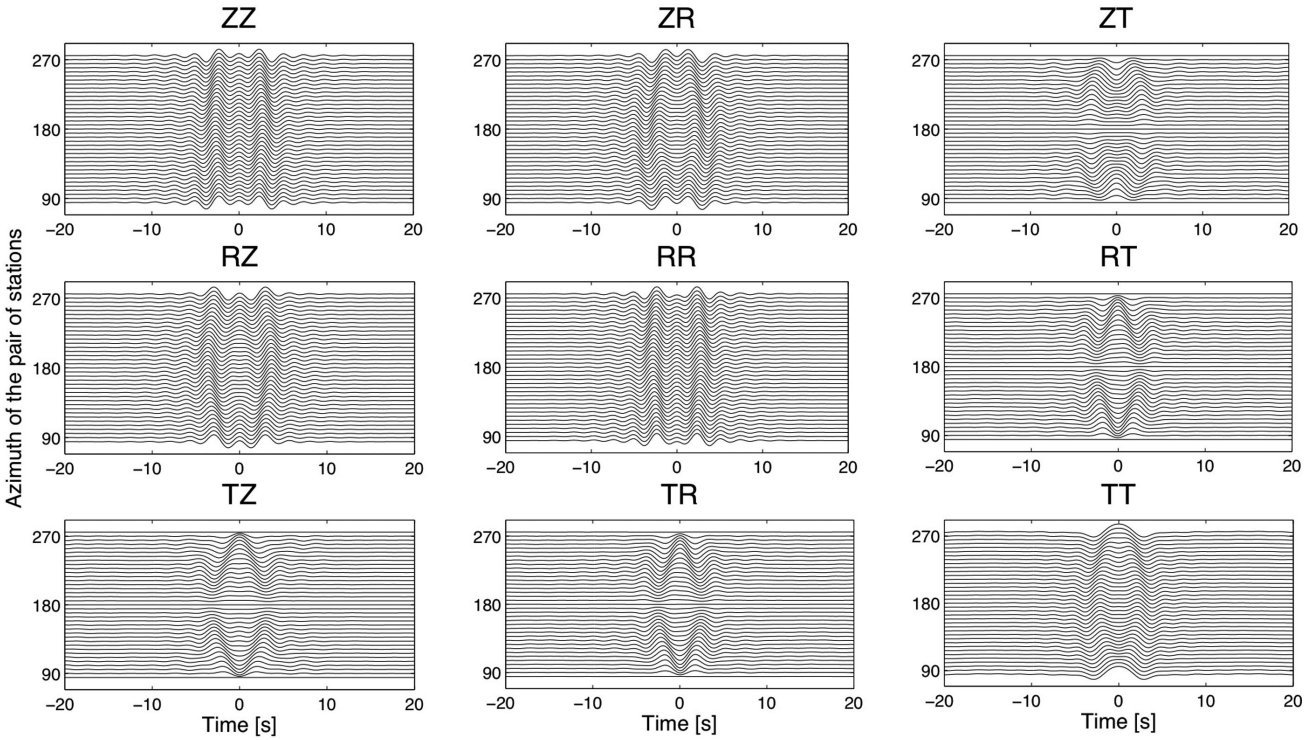

Figure 8. Representation of the nine components of the cross-correlation tensors associated with 37 station-pairs with azimuth going from 90° to 270°. In each panel the bottom signal corresponds to a station-pair of azimuth 90° (parallel to the direction of anisotropy), the middle signal corresponds to a station-pair of azimuth 180° (perpendicular to the direction of anisotropy) and the top signal corresponds to a station-pair of azimuth 270° (parallel to the direction of anisotropy). The source distribution is homogeneous. The difference between the $\delta t/t$ along the slow axis (azimuth 180°) and the fast axis (azimuth 90°) is 20 per cent.

of the noise source distribution (and its variation in the time associated to seasonal changes) should not be a problem since, using beamforming technique (Roux 2009; Durand *et al.* 2011), we can compute the temporal variation of the incidence of the dominant source and then retrieve it from the polarization anomaly given by ORA. A comparison between temporal variation of the polarization anomaly and the seasonal variation of the source incidence is essential to the analysis in order to identify changes of polarization due to anisotropy and the ones due to a source incidence change. Nevertheless, seasonal variations of the source incidence and anisotropy changes do not evolve on the same characteristic time. Hence, a rapid and large change that extends on a relatively small period of time could not be due to a source incidence variation.

The multitude of parameters involved in the creation of ψ_P makes it difficult to find a unique interpretation of the variation of ψ_P. Our numerical experiment shows that ψ_P is highly sensitive to the presence of anisotropy, even for a very shallow anisotropic layer, which is probably not sufficient to affect other physical parameters that produce SWS. In all cases, the angle ψ_P can be very large ($>20^\circ$). The large values of ψ_P with respect to $\delta t/t$ measured for SWS make it easier to consider monitoring ψ_P. Indeed, $\delta t/t$ of SWS can be very small, and even not measurable in some cases; for example, if the anisotropy is weak or if the thickness of the anisotropic layer is small. Another advantage of measuring ψ_P is that monitoring this parameter is possible, as is monitoring seismic anisotropy and observing temporal changes using continuous ambient seismic noise data. As for SWS, it depends on the occurrence of earthquakes, and a temporal change in $\delta t/t$ cannot be observed, as we cannot observe azimuthal changes in SWS in the synthetic experiments presented here. Finally, the last advantage of using CCTs is to deal with $n*(n-1)/2$ measurements for n stations, unlike for n measurements with SWS.

As classically done in ambient noise monitoring, the $\delta t/t$ measurement can also be performed on the surface waves extracted from the CCT. The relative traveltime change ($\delta t/t$) measured on the ZZ component of the CCT of the numerical experiments shows a difference of 20 per cent between the $\delta t/t$ along the slow axis (azimuth 180°) and the fast axis (azimuth 90°; Fig. 8). This value was expected as it corresponds to the velocity difference between the slow axis and the fast axis. However, in practical applications, time delays are not measured on the direct waves extracted from the noise cross-correlations, since the first arrival time delay is subject to seasonal variations. Monitoring relative traveltime is usually performed using the coda of noise cross-correlations (Sabra *et al.* 2005; Brenguier *et al.* 2008). Coda waves are scattered waves that travel large distances and accumulate time delays. Hence, it allows the detection of very small perturbations in seismic velocity. They are also known to be less sensitive to the noise direction than direct waves. On the other hand, the coda is weakly affected by local effects (Planes *et al.* 2014) as expected from a change of anisotropy during an earthquake. Finally, note that typical values of measured $\delta t/t$ in the coda cross-correlations is of the order of 10^{-3} (Brenguier *et al.* 2008).

Durand *et al.* (2011) observed rapid variations ($>20^\circ$) of the horizontal polarization of surface waves at stations of the high resolution seismic network at the moment of the 2004 Parkfield earthquake for only a limited part of the San Andreas Fault. These strong and fast changes occurred only ‘in a small zone in the southern portion of the seismic array, near the San Andreas Fault, and above the primary rupture zone of the Parkfield earthquake’.

Downloaded from https://academic.oup.com/gji/article-abstract/201/2/595/568214 by guest on 22 June 2020

This study provides a possible, and we believe most likely, explanation of these rapid and large horizontal polarization changes in terms of the anisotropic medium. We also note that even if no fast and significant changes of the surface wave polarization were observed in some areas, this does not necessarily mean that the anisotropy distribution did not change. This can be explained by an unfavourable configuration of stations and source, with respect to the direction of the anisotropy, where the polarization is not highly affected.

The Parkfield region is well instrumented and has been well studied. Geophysicists have carried out continuous measurements of the whole area, and preliminary models of the distribution of cracks and the stress field in the region have been obtained. Therefore, the argument of anisotropy change to explain the fast polarization changes can be verified by the measurements of the stress field changes in the area. These measurements were carried out by Nadeau *et al.* (2009) in the analysis of unusual earthquake and tremor seismicity at Parkfield. It appears that the large polarization changes observed by Durand *et al.* (2011) are located in the same zones where Nadeau *et al.* (2009) found the most important regional shear stress changes. This confirms that strong anisotropy changes can induce such strong horizontal polarization anomalies.

6 CONCLUSION

The noise cross-correlation method is a consistent method for monitoring crustal property changes throughout seismic cycles. The ORA procedure applied to the nine-component CCT between two receivers measures the surface wave polarization anomaly angle. Any temporal change in the polarization anomaly angle might be related to seismic anisotropy and a temporal change in the stress field in the medium that induces a change in the crack distribution. The application of this method to synthetic seismograms confirms the hypothesis that anomalous observations of large and fast variations of surface wave polarization with time can be explained by seismic anisotropy. The next step is to apply the noise cross-correlation method to real data, to monitor stress field changes in different tectonic contexts.

ACKNOWLEDGEMENTS

This study is performed in the Seismology Laboratory of Insitut de Physique du Globe de Paris, under the leadership of Jean Paul Montagner and Philippe Roux to whom I would like to express my gratitude for their supervision and guidance. I would like to thank all the co-authors for their collaboration, specially Paul Cupillard for his help with the RegSEM code. The simulations presented in this paper were performed using the Institut de Physique du Globe de Paris Cluster. Many thanks also to Christopher Berrie for the review of the paper.

REFERENCES

Anderson, D.L., 1989. *Theory of the Earth,* Chapter 15: Anisotropy, Blackwell Scientific Publications.

Backus, G., 1962. Long-wave elastic anisotropy produced by horizontal layering, *J. geophys. Res.,* **67,** 4427–4440.

Brenguier, F., Campillo, M., Hadziioannou, C., Shapiro, N.M., Nadeau, R.M. & Larose, E., 2008. Postseismic relaxation along the San Andreas Fault at Parkfield from continuous seismological observations, *Science,* **321**(5895), 1478–1481.

Campillo, M. & Roux, P., 2014. Seismic imaging and monitoring with ambient noise correlations, in *Treatise on Geophysics,* 2nd edn, Vol. 1, pp. 256–271, eds Romanowicz, B. & Dziewonski, A., Elsevier.

Crampin, S., 1981. A review of wave motion in anisotropic and cracked elastic-media, *Wave Motion,* **3,** 343–391.

Crampin, S., 1987. Geological and industrial implications of extensive dilatancy anisotropy, *Nature,* **328,** 491–496.

Crampin, S., Evans, R., Ucer, B., Doyle, M., Davis, J.P., Yegorkina, G.V. & Miller, A., 1980. Observations of dilatancy-induced polarization anomalies and earthquake prediction, *Nature,* **286,** 874–877.

Cupillard, P., Delavaud, E., Burgos, G., Festa, G., Vilotte, J.P., Capdeville, Y. & Montagner, J.P., 2012. RegSEM: a versatile code based on the spectral element methods to compute seicmic wave propagation at the regional scale, *Geophys. J. Int.,* **188**(3), 1203–1220.

Durand, S., Montagner, J.P., Roux, F., Brenguier, F., Nadeau, R.M. & Ricard, Y., 2011. Passive monitoring of anisotropy change associated with the Parkfield 2004 earthquake, *Geophys. Res. Lett.,* **38**(13), doi:10.1029/2011GL047875.

Liu, Y., Zhang, H., Thurber, C. & Roecker, S., 2008. Shear wave anisotropy in the crust around the San Andreas fault near Parkfield: spatial and temporal analysis, *Geophys. J. Int.,* **172**(3), 957–970.

Montagner, J.P., Lognonne, P., Beauduin, R., Roult, G., Karczewski, J.F. & Stutzmann, E., 1998. Toward multiscale and multiparameter networks for the next century: the French effort, *Phys. Earth planet. Inter.,* **108,** 155–174.

Nadeau, R. & Guilhem, A., 2009. Nonvolcanic tremor evolution and the San Simeon and Parkfield, California, earthquakes, *Science,* **325**(5937), 191–193.

Nataf, H.C., Nakanishi, I. & Anderson, D.L., 1986. Measurement of mantle wave velocities and inversion for lateral heterogeneity and anisotropy. III. Inversion, *J. geophys. Res.: Solid Earth (1978–2012),* **91**(B12), 7261–7303.

Planes, T., Larose, E., Margerin, L., Rossetto, V. & Sens-Schoenfelder, C., 2014. Decorrelation and phase-shift of coda waves induced by local changes: multiple scattering approach and numerical validation, *Waves Rand. Complex Media,* **24,** 99–125.

Roux, P., 2009. Passive seismic imaging with directive ambient noise: application to surface waves and the San Andreas Fault in Parkfield, CA, *Geophys. J. Int.,* **179**(1), 367–373.

Sabra, K.G., Roux, P. & Kuperman, W.A., 2005. Emergence rate of the time-domain Green's function from the ambient noise cross-correlation function, *J. acoust. Soc. Am.,* **118**(6), 3524–3531.

Shapiro, N.M., Ritzwoller, M.H. & Bensen, G.D., 2006. Source location of the 26 sec microseism from cross-correlations of ambient seismic noise, *Geophys. Res. Lett.,* **33,** L18310, doi:10.1029/2006GL027010.

Silver, P. & Chan, W., 1991. Shear wave splitting and subcontinental mantle deformation, *J. geophys. Res.: Solid Earth (1978–2012),* **96**(B10), 16 429–16 454.

Stehly, L., Campillo, M. & Shapiro, N.M., 2006. A study of the seismic noise from its long-range correlation properties. *J. geophys. Res.,* **111,** B10306, doi:10.1029/2005JB004237.

Tanimoto, T., 2004. The azimuthal dependence of surface wave polarization in a slightly anisotropic medium, *Geophys. J. Int.,* **156**(1), 73–78.

Vinnik, L.P., 1977. Detection of waves converted from P to SV in the mantle, *Phys. Earth planet. Inter.,* **15**(1), 39–45.

Zhang, H., Liu, Y., Thurber, C. & Roecker, S., 2007. Three-dimensional shear-wave splitting tomography in the Parkfield California, region, *Geophys. Res. Lett.,* **34**(24), doi:10.1029/2007GL031951.

Downloaded from https://academic.oup.com/gji/article-abstract/201/2/595/568214 by guest on 22 June 2020